The cPLA$_2$ C2α Domain in Solution: Structure and Dynamics of Its Ca^{2+}-activated and Cation-Free States

Sameer Varma*†§ and Eric Jakobsson*†‡§¶

*Center for Biophysics and Computational Biology, †National Center for Supercomputing Applications, ‡Department of Biochemistry, §Department of Molecular and Integrative Physiology, and ¶Beckman Institute for Advanced Science and Technology, University of Illinois at Urbana-Champaign, Urbana, Illinois 61801

ABSTRACT Cytosolic phospholipase A_2 is involved in several signal transduction pathways where it catalyses release of arachidonic acid from intracellular lipid membranes. Its membrane insertion is facilitated by its independently folding C2α domain, which is activated by the binding of two intracellular Ca^{2+} ions. However, the details of its membrane-insertion mechanism, including its Ca^{2+}-activation mechanism, are not understood. There are several unresolved issues, including the following. There are two experimentally resolved structures of the Ca^{2+}-activated state of its isolated C2α domain, one determined using x-ray crystallography and the other determined using NMR spectroscopy, which differ from each other significantly in the spatial region that inserts into the membrane. This by itself adds to ambiguities associated with investigations targeting its mechanism of membrane insertion. Furthermore, there is no experimentally determined structure of its cation-free state, which hinders investigations associated with its cation-activation mechanism. In this work, we generate several unrestrained molecular dynamics trajectories of its isolated C2α domain in solution (equivalent to ~60 ns) and investigate these issues. Our main results are as follows: a), the Ca^{2+} coordination scheme of the domain is consistent with the x-ray structure and with previous mutagenesis studies; b), the helical segment of the Ca^{2+}-binding loop, CBL-I, undergoes nanosecond timescale flexing (but not an unwinding), as can be inferred from physiological temperature NMR data and in contrast to low temperature x-ray data; and c), removal of the two activating Ca^{2+} ions from their binding pockets does not alter the backbone structure of the domain, a result consistent with electron paramagnetic resonance data.

INTRODUCTION

The compartmentalization of cells and eukaryotic organelles essentially necessitates the existence of amphitropic molecules, which can reversibly partition from solution into membrane environments. These membrane-docking or lipid-binding molecules often show characteristic tissue distributions and are involved in a large variety of cellular processes. C2 domains are a class of such membrane-targeting protein modules found in a diverse array of signal transducing proteins that regulate key cellular processes at membrane surfaces (for reviews, see (1–10)). These processes include, for example, generation of lipid-derived second messengers, vesicular targeting and fusion, GTPase regulation, protein phosphorylation, pore formation by cytolytic T cells, and ubiquitin-mediated protein degradation. Most of these C2 domains are activated by cytoplasmic Ca^{2+} signals and upon activation dock to specific membrane-associated targets such as phospholipids and in some cases to membrane-bound proteins.

The structures of several (~10) Ca^{2+}-regulated C2 domains, including the C2A domain of synaptotagmin I (Syt-IA), the C2 domain of cytosolic phospholipase A_2 (α-isoform, cPLA$_2\alpha$), and the C2 domain of protein kinase C (PKC), have been determined by x-ray crystallography and/or NMR spectroscopy (11–17). All these C2 domains share a common structural motif in which they fold into two separate four-stranded β-sheets that pack against each other to form a sandwich. At one edge of this β-sandwich, three interstrand loops, termed CBL I–III in order of their sequence in the primary structure, form the binding clefts for the activating Ca^{2+} ions. The Ca^{2+}-loaded C2 domains characterized to date possess from one to three Ca^{2+} ions bound in different combinations of these binding sites (13,16,18–20).

Despite this strong structural similarity, the Ca^{2+}-activated states of these domains do not in particular share a common membrane-docking mechanism. Evidence supporting the roles of three different mechanisms exist (2,5,6,15,21–28): a), the hydrophobic interaction mechanism in which the binding of Ca^{2+} ions neutralizes the membrane-docking region of the domain and enhances in interaction with zwitterionic membranes, b), the electrostatic switch-activation mechanism in which the binding of Ca^{2+} ions alters the electrostatic potential at the docking region to the extent that it increases its attraction to acidic (negatively charged) phospholipids, and c), the coordinating lipid-activation mechanism in which the bound Ca^{2+} ions directly coordinate with lipid molecules. However, to date there are no fine-grained models that can isolate and quantify the roles played by each of these interactions (electrostatic, hydrophobic, and chelation) in the membrane docking of these domains.

Here we carry out investigations to understand both the Ca^{2+}-activation and the membrane-insertion mechanisms

Submitted June 20, 2006, and accepted for publication October 13, 2006.

Address reprint requests to Eric Jakobsson, Tel.: 217-244-2896; Fax: 217-244-2909; E-mail: jake@ncsa.uiuc.edu.

Sameer Varma's and Eric Jakobsson's present address is Sandia National Laboratories, MS-1413, PO Box 5800, Albuquerque, NM 87185.

© 2007 by the Biophysical Society

0006-3495/07/02/966/11 $2.00

doi: 10.1529/biophysj.106.091850

of the C2α (C2) domain of $cPLA_2$. $cPLA_2$ is involved in the catalytic release of arachidonic acid from cellular phospholipids, which is subsequently used for biosynthesis of eicosanoids (prostaglandins, leukotrienes, and others). It is regulated in multiple pathways, including those that control Ca^{2+} ion concentrations, or those that control enzyme phosphorylation states, and even those that control $cPLA_2$ protein levels, and is used to exert both rapid and prolonged effects on cellular processes, such as inflammation. $cPLA_2$ is rapidly activated by increased intracellular Ca^{2+} concentrations and phosphorylation by MAP kinase. The membrane insertion of $cPLA_2$ is however triggered only by the binding of two intracellular Ca^{2+} ions to its C2 domain (2,6,19,29,30). Once its C2 domain binds two Ca^{2+} ions, the Ca^{2+}-bound portion of the domain, including the Ca^{2+}-binding loops (CBL I–III), inserts into the membrane interior (2).

The molecular-level details of its Ca^{2+}-activation and membrane-insertion mechanisms are, however, not completely understood and are currently hampered by several unresolved issues that also include the following. To date, two high-resolution structures of its isolated Ca^{2+}-activated state exist (12,16). One of these structures was determined using x-ray crystallography, whereas the other was determined using NMR spectroscopy. These structures are mostly similar to each other, except with respect to the details of the spatial region that has been suggested (2) to interact with lipid groups during membrane insertion (see Fig. 1). Undoubtedly, structural ambiguities associated with this spatial region of the domain can easily be expected to trickle down further into any investigations aimed at probing the molecular level details of its interaction with membranes and therefore warrants further investigations of the dynamics of its calcium-activated state in solution. This knowledge can also serve as a benchmark for isolating its structural and dynamical changes associated solely with membrane insertion. Another issue that in particular hampers investigations regarding its Ca^{2+}-activation mechanism is the unavailability of experimental structural information on its cation-free (apo-) state. An understanding of its calcium-activation mechanism would clearly benefit from knowledge of the dynamics of its cation-free state in solution. To address these issues of Ca^{2+} activation and membrane insertion, we generate several molecular dynamics (MD) trajectories (equivalent to a total simulation time of ~60 ns) of the isolated C2 domain of $cPLA_2$ in solution, both in the presence and in the absence of the activating Ca^{2+} ions.

METHODS

All MD trajectories were generated using the GROMACS (version 3.1.4) modeling software (31). The coordinates of the C2 domain of $cPLA_2$ were taken from the x-ray crystal structure (Protein Data Bank (PDB) code: 1RLW) (12). All hydrogen atoms belonging to the optimized potential for liquid simulations-all atom (OPLS-AA) force field (32) were added using PDB2PQR (33), followed by a subsequent optimization of the global hydrogen-bond network (28,33). The starting configuration of each trajectory was generated as follows: The protein was first translated to the center of a rectangular box (dimensions, 8.5 × 6.5 × 6.5 nm). The box was then filled with water molecules (~11,000) using the GROMACS utility program Genbox. The C2 domain by itself, i.e., without any of the crystallographically resolved Ca^{2+} ions, and assuming default protonation states for all titratable residues, carries a net charge of −8 eu. Thus, some water molecules were then substituted (selected randomly) with an appropriate combination of anions (Cl^-) and cations (Ca^{2+}) to neutralize the charge of the system (protein and water), the maximum number of substitutions being 16 (8 Ca^{2+} and 8 Cl^-) in the case of the simulation of the apo-state of the domain in CaCl. The system was then subjected to a 10-ps-long MD simulation at a temperature of 100 K using an integration time step of 1 fs. The final snapshot of this simulation was then subjected to another 10-ps-long MD simulation at a higher temperature of 200 K and using an integration time step of 2 fs. The final snapshot of this simulation was then used as the starting configuration for simulation at 300 K. For all such short MD simulations that were carried out at temperatures lower than 300 K, we found that 10 ps was enough time to allow for stabilization of simulation box size.

For each simulation from which we gathered and report data we used the following: NPT conditions; a temperature of 300 K; a pressure of 1.03 bar; a Nosé-Hoover algorithm (34) with a coupling constant of 0.2 ps to maintain temperature; a Parrinello-Rahman method (35) with a coupling constant of 1 ps to maintain boundary pressure conditions; particle mesh Ewald with Fourier spacing of 0.15 nm, a sixth-order interpolation and a 1.0-nm cutoff in direct space for long-range electrostatic corrections; a 1.0-nm cutoff for van der Waal interactions, unless specified otherwise; an integration time step size of 2 fs; the LINCS algorithm (36) to constrain all bond lengths; the SETTLE algorithm (37) for constraining bond lengths in water molecules; an all-atom OPLS force field (32) for protein; and a simple point charge (SPC) model to describe water molecules, unless otherwise specified. We understand that the lack of a polarizable force field will introduce numerical errors in interactions involving Ca^{2+} ions. However, the broad phenomena

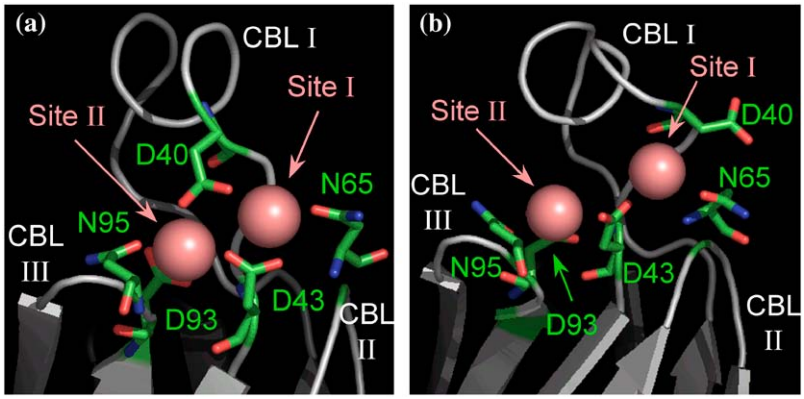

FIGURE 1 Partial view of the structure of the C2 domain of $cPLA_2$ determined using (*a*) x-ray crystallography (12), and (*b*) NMR spectroscopy (16). The β-sheets are drawn as cartoons, the three CBLs are drawn as ribbons, and the coordinating side chains are highlighted as stick models. This spatial region of the domain binds Ca^{2+} ions and is also involved in membrane docking (2). We note two main differences between the structures obtained using x-ray crystallography and NMR spectroscopy: 1), the roughly helical segment of CBL-I in the NMR structure is a well-defined α-helix in the x-ray structure, and 2), the side chain of residue Asp-40 does not coordinate with either of the activating Ca^{2+} ions in the NMR structure as it does in the x-ray structure. This figure was made using PyMol (DeLano Scientific, Palo Alto, CA).

we observe in these simulations appear sufficiently robust and are not likely to be compromised by that degree of inaccuracy.

The MD simulations were performed on the Intel Xeon Linux and the Intel Itanium 2 Linux clusters provided by the National Center for Supercomputing Applications at the University of Illinois, Urbana-Champaign.

RESULTS AND DISCUSSIONS

There are at present two experimentally determined structures of the isolated Ca^{2+}-activated form of $cPLA_2$ C2 domain: 1), a low temperature (100 K) structure determined using x-ray crystallography (12) and; 2), a physiological temperature (308 K) solution structure determined using NMR spectroscopy (16). Fig. 1 illustrates the spatial region of each of these two structures that has been identified (2) to interact with lipid during membrane insertion. It comprises mainly the three CBLs, CBL-I, CBL-II, and CBL-III, and the Ca^{2+}-binding cleft. Below we discuss the differences between these two structures.

One difference between the x-ray structure and the NMR structure in Fig. 1 is associated with the backbone structure of CBL-I. We find that the segment of CBL-I, which is a well-defined α-helix in the x-ray structure, is only roughly helical in the NMR structure. Fig. 2 compares this helical segment of CBL-I in the two structures from a different visual perspective, highlighting backbone atoms of residues involved in the formation of intramolecular hydrogen bonds. In the x-ray structure, we see that the G-33.O atom is hydrogen bonded to the D-37.N atom, the A-34.O atom is hydrogen bonded to the M-38.N atom, the F-35.O atom is hydrogen bonded to the L-39.N, and the G-36.O is hydrogen bonded to the D-40.N atom. This hydrogen-bonding pattern between the backbone atoms of the ith and the $(i + 4)$th residues indicates that it is a well-defined α-helix. In contrast, we find that in the NMR structure, only two backbone atoms, the backbone nitrogen of Ala-34 and the backbone oxygen atom of Met-38, are within hydrogen-bonding distance from each other, indicating that it is not an α-helix.

A further difference between the x-ray and NMR structures is associated with the coordination scheme adopted by the C2 domain to bind Ca^{2+} ions. From Fig. 1, we can see that in the x-ray structure (12) the two activating Ca^{2+} ions occupy adjacent binding sites, I and II, and coordinate with five amino acid side chains. These amino acid side chains provide either one (monodentate) or two (bidentate) coordinating oxygens: Asp-40 (bidentate, bridging Ca^{2+} I and II), Asp-43 (bidentate, bridging Ca^{2+} I and II), Asn-65 (monodentate, Ca^{2+} I), Asp-93 (bidentate, Ca^{2+} II), and Asn-95 (monodentate, Ca^{2+} II). In contrast, the NMR data (16) indicate that on average, only four of these five side chains coordinate with the two activating Ca^{2+} ions. In particular, Asp-40 does not coordinate with either of the activating Ca^{2+} ions in ~80% of the substructures. In a site-directed mutagenesis-based study (28), it was found that a substitution of any of these five coordinating side chains to a cysteine side chain resulted in decreasing the Ca^{2+}-binding affinity of the domain, with the N-95C mutation having the least effect on Ca^{2+}-binding (an approximately threefold decrease) and a D-43C mutation resulting in a complete loss of Ca^{2+} affinity. It was also found that a D-40C mutation resulted in an ~21-fold loss in binding affinity and a complete inactivation of one of the binding sites, supporting the hypothesis that it is indeed involved in coordinating with the bound Ca^{2+} ions. We therefore used the crystallographically derived Ca^{2+}-activated structure of the domain as the starting point for all the MD simulations in this work.

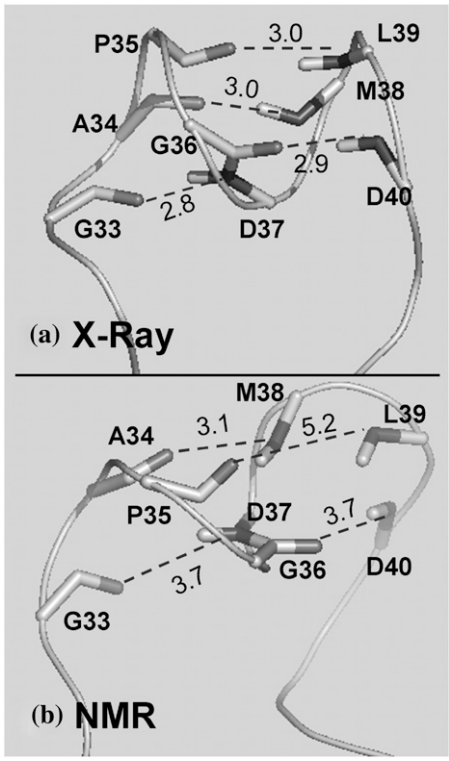

FIGURE 2 The structure of the helical segment of CBL-I as determined using (*a*) x-ray crystallography (12). The helical segment is drawn as a ribbon and the backbone atoms involved in intramolecular hydrogen bonds are highlighted as stick models. The hydrogen bonds between the backbone atoms of the ith and the $(i + 4)$th residues are drawn as dashed lines, and the distances between the proton donor and acceptor atoms are indicated in angstrom units. (*b*) NMR spectroscopy (16). The corresponding proton donors and acceptor atoms are shown and the distances between these atoms are also indicated in angstrom units. This figure was made using PyMol.

Ca^{2+}-activated state of the C2α domain

In this section, we report on results obtained from MD trajectories generated for the Ca^{2+}-activated structure of the domain. In a 10-ns-long MD trajectory of the domain generated in explicit solvent, we find that each of the bridging side-chain residues, i.e., Asp-40 and Asp-43, coordinate with both Ca^{2+} ions throughout the entire course of the trajectory. We also find that Asp-93 does not at any point in the trajectory coordinate with the calcium ion in site I, a result consistent with both crystallographic (12) and

NMR (16) data. We also find that the monodentate side chains, Asn-65 and Asn-95, coordinate with only their respective Ca^{2+} ions in sites I and II. We also note that unlike the coordinating side chain of Asn-65, the coordinating side chain of Asn-95 does not coordinate with its Ca^{2+} ion throughout the entire course of its trajectory. The coordinating side chain of Asn-95 undergoes continuous fluctuations throughout the simulation such that at some instances it is within coordinating distance from the Ca^{2+} ion in site II and at other instances it is not. This is illustrated in Fig. 3 via a superimposition of snapshots taken at every 0.5 ns of the MD trajectory. This result is in fact consistent with previous mutagenesis studies (28), which revealed that the side chain of Asn-95 plays a less significant role than the side chain of Asn-65 in Ca^{2+} binding. In those experiments, a N-95C mutation had resulted in an approximately threefold loss in Ca^{2+}-binding affinity, whereas a N-65C mutation had resulted in an approximately ninefold loss in Ca^{2+}-binding affinity. In essence, we find that the coordination scheme of the two activating Ca^{2+} ions as seen in the x-ray crystal structure is well maintained throughout the course of the simulation.

Table 1 shows the root mean square (RMS) deviations of backbone atoms belonging to different segments of the domain, with different models of water employed in the simulation. We find that the majority of the secondary structure of the domain predicted by the crystallographic data is maintained. We also note that CBL-I has the highest RMS deviation among the three CBLs.

The RMS fluctuations of the backbone atoms of the domain are shown in Fig. 4. As expected, we find that the backbone atoms belonging to the β-sheets undergo lower RMS fluctuations than those belonging to the loops. However, we find that the backbone atoms belonging to the short two-turn helix in CBL-I undergo the highest RMS fluctuations among all the other backbone atoms of the domain. An investigation of the MD trajectory of the backbone atoms of the CBL-I reveals that these large fluctuations correspond to a flexing of this helix but not an unwinding of the helix as reported in cases of other Ca^{2+}-binding proteins such as calmodulin (38). We find that the hydrogen bonds between the backbone proton donor (nitrogen) and acceptor (oxygen) atoms of the helical segment of CBL-I (illustrated in Fig. 2) periodically break and re-form during the simulation. The evolution of distances between these four acceptor oxygen atoms and their corresponding donor nitrogen atoms in this MD simulation are plotted in Fig. 5 *a*, for the simulation with the SPC water model. We find that at any given instance of the simulation, none of these four proton donors stay simultaneously within hydrogen-bonding distances from their corresponding acceptors. Instead, and especially in the cases of the proton donors of residues L-39 and D-40, we see that on several occasions they approach within hydrogen-bonding distances of their corresponding acceptors in residues F-35 and G-36 for nanosecond timescale intervals and move away from them during other time intervals. Essentially, we find that at a given instance of the entire trajectory, there is at

TABLE 1 Average RMS deviations (in angstrom units) of backbone atoms belonging to different segments of the C2 domain computed from 10-ns-long MD trajectories generated using different water models: SPC, SPC/E, and TIP4P

Segment	Residue ID	SPC	SPC/E	TIP4P
CBL-I	29–43	1.5	1.4	1.4
CBL-II	50–72	1.0	1.0	1.0
CBL-III	94–99	0.7	0.7	0.5
β-sheets	–	1.2	0.9	1.0

We find that irrespective of the water model used in these simulations, the backbone atoms belonging to the CBL-I undergo the highest RMS deviation from their x-ray coordinates.

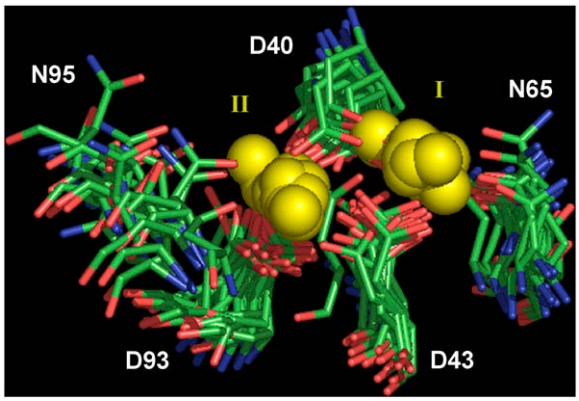

FIGURE 3 Coordinating side chains in the Ca^{2+}-binding cleft of the domain. Snapshots were taken at every 0.5 ns of a 10-ns-long MD simulation of the cPLA$_2$ C2 domain and superimposed over each other. The side chains are drawn as stick models and the Ca^{2+} ions are drawn as spheres. We find that the crystallographic coordination scheme is maintained throughout the course of the simulation. This figure was made using PyMol.

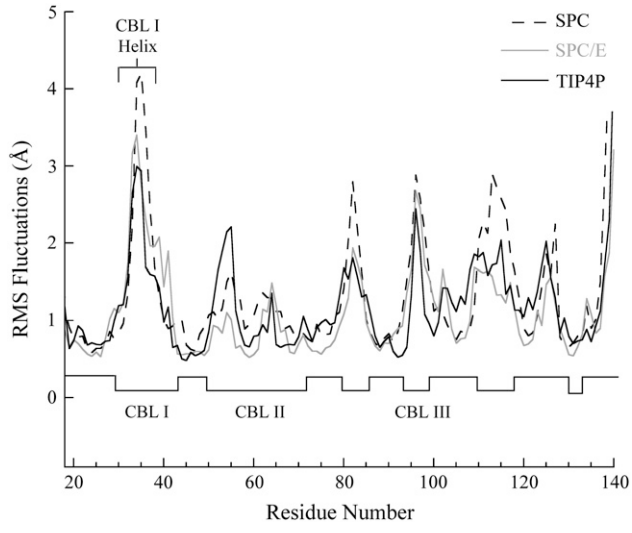

FIGURE 4 RMS fluctuation of backbone atoms of the cPLA2 C2 domain. SPC, SPC/E, and TIP4P refer to RMS fluctuations of backbone atoms computed from 10-ns-long MD trajectories generated using those water models.

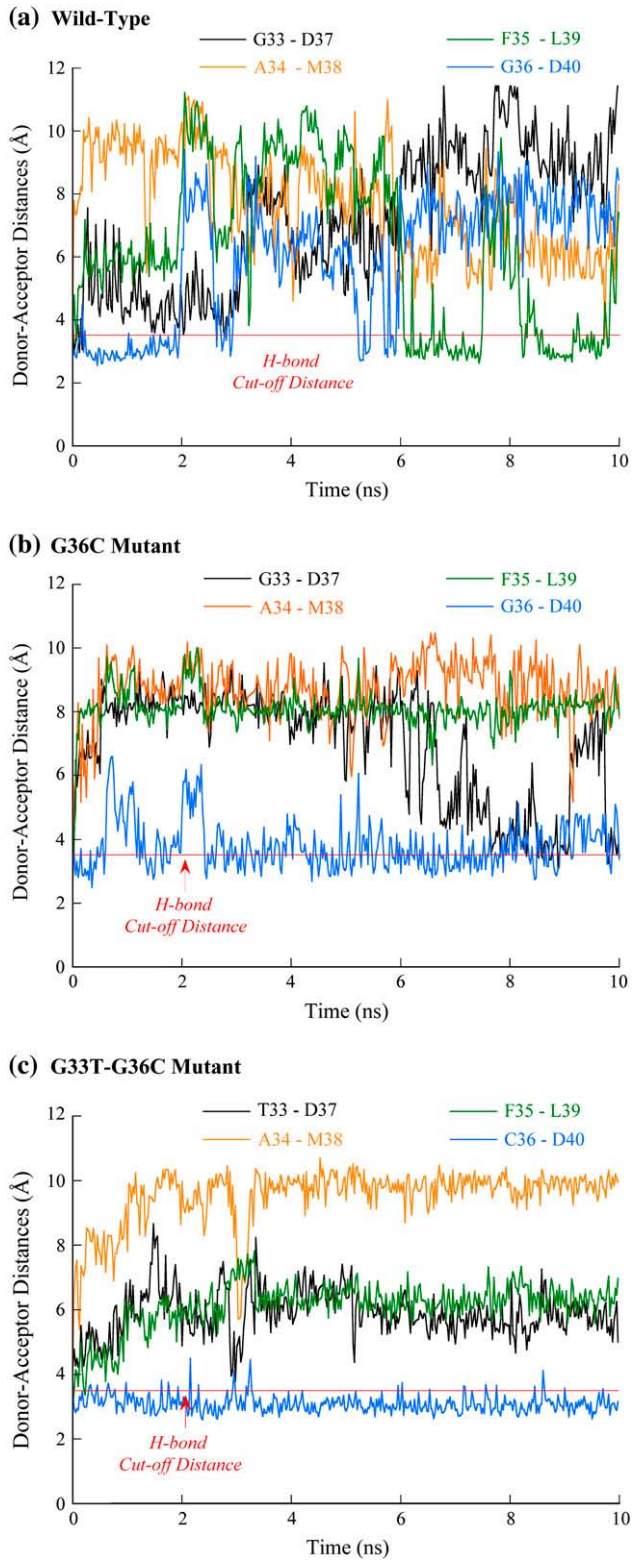

FIGURE 5 Time series of the distances between the four proton donor atoms (backbone nitrogens) and the four corresponding acceptor atoms (oxygens) belonging to the helical region of CBL-I. These distances were computed at every 10 ps of a 10-ns-long MD simulation of the $cPLA_2$ C2 domain in solution. (*a*) Wild-type domain. (*b*) G-36C mutant. (*c*) G-33T-G-36C mutant.

most one proton donor within hydrogen-bonding distance from its corresponding acceptor. This result is reflective of the average NMR structure (16) of the helical segment of CBL-I, where only one proton donor is within hydrogen-bonding distance from its corresponding acceptor. This MD simulation however does not predict the same proton donor to be within hydrogen-bonding distance from its corresponding acceptor that was predicted by the NMR data, which may be due to the relatively small sampling time of the MD simulation when compared against the dwell time of a proton donor near its corresponding proton acceptor. Together, we find that the structural dynamics of CBL-I are more consistent with the NMR data than with the crystallographic data.

We find that this nanosecond timescale flexing of the helical segment of CBL-I is due to the presence of the two glycine residues, Gly-33 and -36. Note that Gly-33 is located at the N-terminus of the helical segment, and Gly-36 is located halfway through the helical segment. The Ramachandran plots of these glycines computed from this 10-ns-long MD trajectory are shown in Fig. 6. We find that in the given environment, the backbone torsional angles of Gly-36 show no specific preference toward forming either a left-handed or a right-handed helix, and the backbone torsional angles of Gly-33 show a higher preference toward forming a left-handed helix. As control experiments, we generated two other 10-ns-long MD trajectories of the domain using the same environmental variables, but in one simulation we mutated Gly-36 to a cysteine residue (G-36C mutant) and in the other simulation, we mutated both glycine residues to residues having bulkier side chains: Gly-33 to a threonine and Gly-33 to a cysteine (G-33T-G-36C mutant). We found that the G-36C mutation reduced the flexing of the helical segment, especially at its C-terminal, whereas the G-33T-G-36C double mutation completely removed the nanosecond timescale flexing of the helical segment. However, neither of these two mutations resulted in a simultaneous stabilization of the four intramolecular hydrogen bonds. We found that in the simulation conducted with the G-36C mutation (Fig. 5 *b*), the hydrogen bond between the backbone atoms of residues Phe-35 and Leu-39 broke within the first nanosecond of the trajectory and stayed broken throughout the trajectory. And in the simulation conducted with the double mutation (Fig. 5 *c*), three of the four hydrogen bonds, i.e., between the backbone atoms of Ala-34 and Met-38, the backbone atoms of Phe-35 and Leu-39, and the backbone atoms of Tyr-33 and Asp-37, broke within the first nanosecond of the trajectory and stayed broken throughout the trajectory. An investigation of the backbone torsional angles indicates that the residues belonging to the helical segment continue to adopt a helical structure despite these tethered intramolecular hydrogen bonds. Essentially, we find that the mutations of the glycines to residues that have bulkier side chains results in decreasing the flexing of the helical segment of CBL-I. The reason that some of the backbone hydrogen bonds break in all these three simulations is perhaps a consequence of

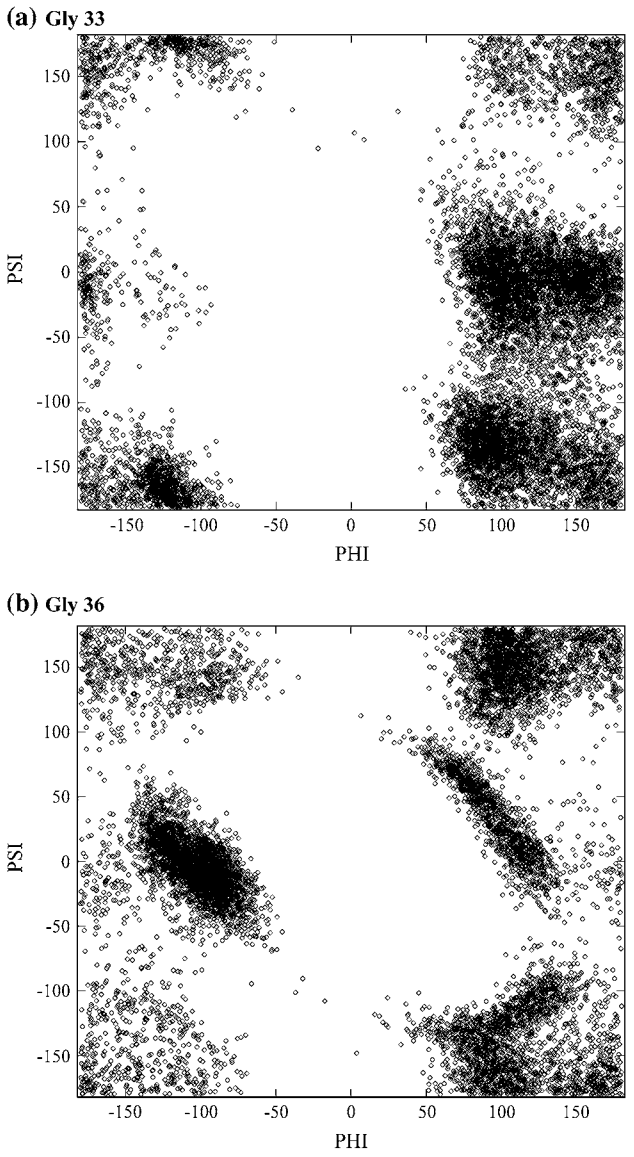

FIGURE 6 Ramachandran plots of the two glycine residues, G-33 and G-36, found in the helical segment of CBL-I of the cPLA2 C2 domain. These Ramachandran plots were computed from a 10-ns-long MD simulation of the domain in solution.

their exposure to water, which competes with these backbone hydrogen acceptors and donor atoms for hydrogen bonding (see below).

To ascertain that this flexing of the helical segment in CBL-I was not an artifact of the SPC water model (39) used in this simulation, we carried out two other 10-ns-long MD simulations of the wild-type domain in explicit solvent. In one simulation, we used a simple point charge-extended (SPC/E) water model (40), and in the other simulation we used a TIP4P water model (41). The RMS deviations of backbone atoms computed from these simulations are listed in Table 1, and the RMS fluctuations of backbone atoms computed from these simulations are included in Fig. 4. We find that the RMS fluctuations and the RMS deviations of the corresponding CBLs in the three simulations are slightly different from each other and so are the corresponding proton donor-acceptor distance dynamics of the backbone atoms of the helical region of CBL-I (data not shown). This is expected, as these three water models agree with each other and with experiments in reproducing such physical properties like average configurational energies (42–44) but differ from each other in reproducing other important physical properties like isotropic dielectric constants (42,43) and self-diffusion constants (45). (For a comprehensive review of properties of water models see Guillot (46)). The important point is that whatever the water model, the helical segment of CBL-I undergoes flexing.

We also tested the effect of some other simulation parameters on the flexing of the helix. In all the above MD simulations, we used an OPLS-AA (32) force field for proteins. Normally, when using an OPLS-AA force field for proteins, Lennard-Jones (LJ) interactions are truncated beyond a distance of ~1.0 nm (32). This is because LJ interactions decay as a sixth-order function. However, beyond the cutoff distance these LJ interactions, although seemingly very small, are always attractive. Omitting these attractive interactions beyond a 1.0-nm distance has been shown to decrease density of lipid bilayers (S. W. Chiu and E. Jakobsson, unpublished) and therefore may have resulted in the flexing of the helix. To ascertain that the decrease in the helicity of CBL-I seen in these simulations was not a result of these LJ cutoff lengths, we generated a separate 3-ns-long MD trajectory of the calcium-activated wild-type domain not only using a higher LJ cutoff of 16 Å but also enforcing LJ pair list updates at every integration time step. We did not see any systematic effect on the helicity of CBL-I.

In essence, we find that the helical segment of CBL-I (in wild-type domain) undergoes nanosecond timescale flexing, and its average structure is consistent with NMR data, rather than the low temperature (100 K) x-ray data. This difference between the x-ray and NMR (or MD) structures of CBL-I is perhaps due to the differences between the environmental conditions of x-ray crystallography and solution NMR spectroscopy (or these MD simulations). It is well known that the propensity for formation of an α-helix is influenced by its degree of exposure to water, as well as local temperature (see for example (47–51)). Thermal fluctuations can cause local opening and closing of backbone CO-NH hydrogen bonds, and if the local environments of such hydrogen bonds are not shielded from water, as in this case, water molecules can compete for hydrogen bonding with backbone donors and acceptors and decrease their stability. The x-ray crystallization conditions of low temperature can be expected to decrease both the rate and magnitude of opening and closing of backbone CO-NH hydrogen bonds and thereby stabilize them to a larger extent in comparison with physiological conditions, as present in NMR experiments or in our current MD simulations. In the very same context, it is interesting to

note that during membrane insertion, time-resolved fluorescence resonance energy transfer (FRET) studies have identified (2) CBL-I to lie at the interface of lipid tails and lipid headgroups, which is an environment where one can expect a reduced exposure of its helical segment to water and therefore provide for conditions that increase the propensity of the formation of a well-defined α-helix.

Coordinating side chains in the apo-state

The structure of the apo-state of the C2α domain, that is, the structure of the C2 domain without any bound cations, is not known. Nevertheless, in the absence of Ca^{2+} ions in the binding cleft, it is easy to argue that the high density of negative charges in the binding cleft created by three aspartates (D-40, D-43, and D-93) and two asparagines (N-65 and N-95) would result in a complete disruption of the binding pocket. This appears to be a very likely scenario, especially because all these side chains belong to flexible loops CBL-I, CBL-II, and CBL-III (illustrated in Fig. 1). However, electron paramagnetic resonance (EPR) studies have shown that the Ca^{2+}-binding event triggers only small and localized changes in the dynamics of these coordinating loops (2). Therefore, it had previously been hypothesized (28) that some of these coordinating aspartates may be protonated in the absence of any cations in the binding cleft and that the neutrality of these aspartates might be preventing the loops from undergoing any large conformational changes upon Ca^{2+} binding.

To test this hypothesis, we generated three separate MD trajectories, differing only in the definition of the water model. One simulation was carried out with SPC water (39), one with SPC/E water (40), and one with TIP4P water (41). Each of these trajectories was initiated after removing the crystallographically resolved Ca^{2+} ions from the binding cleft and setting the three aspartates (D-40, D-43, and D-93) to be fully charged. All these simulations were carried out in the presence of eight Ca^{2+} and eight Cl^- ions, roughly corresponding to a Ca^{2+} concentration of 40 mM, and balancing the C2 domain net charge of -8 eu, so that the entire system is electroneutral. In such a situation, we note that the concentration of the Ca^{2+} ions necessary to balance the negative charge of the C2 domain is quite high, whereas in the EPR experiments on the apo-state, the calcium concentration is kept very low by the chelator EDTA to ensure observation of the apo-state. In our system, we ensure sampling of only a true apo-state by employing the following strategy: we tracked the distance of each Ca^{2+} ion in the simulation box from the side-chain carboxylate carbon atom (Cγ) of Asp-43 and collected MD data only up to the point when no Ca^{2+} ions were within 15 Å ($>$ Bjerrum length at 300 K) from this atom. Because data obtained from all these simulations were qualitatively similar, we present data only from the simulation that was generated with SPC (39) water. We were able to sample data up to the first 1.6 ns of the trajectory, before a calcium ion drifted too close to the binding site.

As can be seen from Fig. 7, the RMS deviations of backbone atoms from the crystal structure in all the three loops remained similar to those that were observed for the Ca^{2+}-activated state. Clearly, the removal of Ca^{2+} ions from the binding cleft was not accompanied by any rearrangements of the backbone. This implies that in the absence of bound Ca^{2+} ions in the binding cleft, the large electrostatic repulsive forces between the negative charges of the three aspartates are entirely negated via a combination of screening by the water in the cavity and side-chain rearrangements. To identify these side-chain rearrangements, we first calculated the RMS deviations of the side chains of all the residues that were coordinating the Ca^{2+} ions in the crystal structure, i.e., Asp-40, Asp-43, Asp-93, Asn-65, and Asn-95. We found that residue Asp-43 showed the least RMS deviation (<1 Å) among all these residues. So we then plotted the distances of the charge groups on these residues, that is, the carboxyl group on the aspartates, the amine group on asparagines, and the carbonyl group on asparagines, from the carboxyl group of Asp-43 as a function of time. Fig. 8 (separate plots) shows the evolution of these distances during the course of the 1.6-ns-long trajectory. We find that the side chains of both asparagines (N-65 and N-95) have rotated such that in the absence of any Ca^{2+} ions, their amino groups now face the empty cation-binding cleft. This is illustrated in Fig. 9 using a 1-ns snapshot of the MD trajectory. These rotations allow them to electrostatically interact with the aspartates in the binding cleft (Asn-65 with Asp-43, and Asn-95 with Asp-93) and relieve the electrostatic energy of the binding cleft. Simultaneously, the side chain of residue Asp-40 moves away from the rest of the charge groups in the binding cleft, which increases the size of the cavity. This allows water to shield the interaction between Asp-40 and the other two aspartates, Asp-43 and -93. These three side-chain motions effectively reduce the repulsive forces between the charged aspartates without any rearrangements of the protein backbone. Interestingly, we find that these side-chain rearrangements occur almost instantaneously, within the 20 ps of equilibration carried out at lower temperatures.

We interpret this result based on the assumption that a 1.6-ns-long simulation is enough to capture any transitions in the torsion angles of the protein backbone in the vicinity of the cleft. We believe this is a reasonable assumption, because only a single nanosecond long MD trajectory of the apo-state of the C2 domain of protein kinase C_β was reported to result in significant backbone rearrangements of its Ca^{2+}-binding cleft (52).

Together, we find that the removal of Ca^{2+} ions from the binding cleft produces no noticeable backbone rearrangements, a result consistent with EPR data (2) and obtained despite considering all the three aspartates, D-40, D-43, and D-93, to be in their fully charged states.

CONCLUSIONS AND SUMMARY

The specific conclusions we draw from the unrestrained dynamics of the C2 domain of $cPLA_2$ in solution are

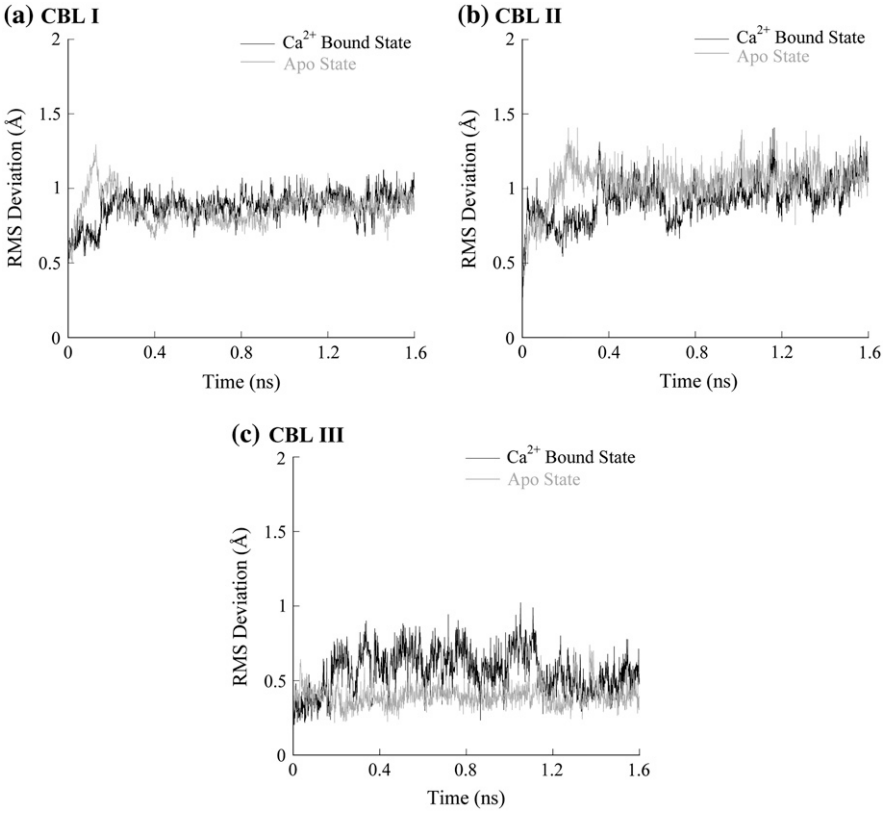

FIGURE 7 Time series of the RMS deviation of the backbone atoms of CBLs of the domain. The RMS deviation profiles of (*a*) CBL-I, (*b*) CBL-II, and (*c*) CBL-III, computed from the simulation of the cation-free state of the domain are compared to their corresponding RMS deviation profiles computed from the simulation of the Ca^{2+}-bound state of the domain.

1. In the Ca2+-activated state, the coordination complex as revealed by the low temperature x-ray structure (12) is maintained throughout the course of the simulation. We also note that unlike the coordinating side chain of monodentate Asn-65, the coordinating side chain of monodentate Asn-95 undergoes continuous fluctuations throughout the simulation such that at some instances it is within coordinating distance from the Ca2+ ion in site II and at other instances it is not. This result is consistent with previous mutagenesis studies (28), which revealed that the side chain of Asn-95 plays a less significant role than the side chain of Asn-65 in Ca2+ binding.
2. In the Ca2+-activated state, the short two-turn helical segment of CBL-I is not likely to be a well-defined α-helix under physiological conditions, a result consistent with NMR data (16) and different from x-ray data (12).
3. In the Ca2+-activated state, the helical segment of CBL-I undergoes nanosecond timescale flexing. This nanosecond timescale flexing is due to the presence of two glycine residues, Gly-33 and -36, that make up the helical segment. We find that a simultaneous substitution of these glycines to amino acids having bulkier side chains completely eliminates this flexing. FRET studies (2) have shown that CBL-I belongs to the region of the domain that inserts into the lipid bilayer during membrane insertion. It is therefore possible that these glycine residues play a vital role in the process of membrane insertion by imparting flexibility to CBL-I. In this context, we note general evidence of the functional significance of protein flexibility or ''intrinsic disorder'' (53) and particular evidence for the role of functional disorder in protein-protein association triggered by Ca2+ binding (54). Based on the results of our work, we suggest as a hypothesis to be tested in future work that protein flexibility also plays a role in Ca2+-mediated protein-lipid association. Furthermore, we also hypothesize that the functional role of the flexibility is to also provide for a transient exposure of CBL hydrophobic side chains on the protein surface, thus facilitating association with the membrane. This hypothesis will be explored in future studies of membrane association with the Ca2+-bound state.
4. We find that when we introduce pseudotorsional restraints into the helical portion of CBL-I via point mutations, we eliminate the nanosecond timescale flexing of the helix, but this still does not result in the formation of a well-defined α-helix. This is most likely due to the exposure of CBL-I to water under conditions of physiological temperatures. It is well known that thermal fluctuations can cause local opening and closing of backbone CO-NH hydrogen bonds, and if the local environments of such hydrogen bonds are not shielded from water, as in this case, water molecules can compete for hydrogen bonding with backbone donors and acceptors and decrease their stability (47–51). This is also supported

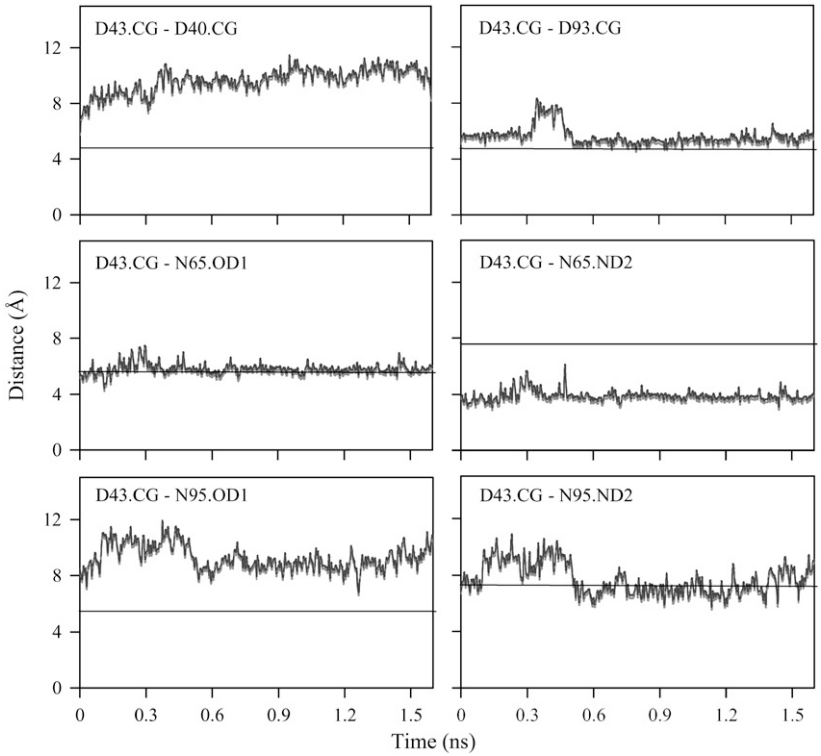

FIGURE 8 Evolution of the distances of the side-chain amino and carbonyl groups of residues Asn-65 and Asn-95, and the side-chain carboxylate groups of Asp-40 and Asp-93 from the side-chain carboxylate of Asp-43.

by the observation that the dynamical details of the helical segment of CBL-I are dependent on the water model used for simulating the domain in solution (see Fig. 4).

5. We find that removal of both bound Ca2+ ions from the crystal structure does not result in altering the backbone structure of the domain, a result consistent with EPR data (2). We find that the large electrostatic repulsive forces between the negative charges in the binding cleft were negated via three well-defined side-chain rearrangements: χ-angle rotations involving the side chains of the two asparagines (Asn-65 and -95) and a movement of residue Asp-40 away from the binding cleft.
6. The side chains coordinating with the bound Ca2+ ion in the crystal structure belong to flexible loops CBL-I, CBL-II, and CBL-III. Therefore, in the absence of the activating Ca2+ ions in the binding cleft it seemed plausible (28), before the simulations presented in this work, to argue that the high density of negative charges in the binding cleft created by three aspartates (D-40, D-43, and D-93) and two asparagines (N-65 and N-95) would result in a disruption of the binding pocket structure. However, in this study we find that MD trajectories generated upon removal of both bound Ca2+ ions from the crystal structure and setting all the three aspartates to be fully charged results in no changes in the secondary structure of the domain. We therefore now find no reason to believe that any of these aspartates would be protonated in the apo-state of the domain. These aspartates are exposed to solvent in the apo-state, which suggests only minor shifts from bulk titration state values (55), and charging them simultaneously does not result in any backbone rearrangements of the domain, consistent with EPR data (2).
7. Our inference from these simulations, that the three aspartates in the binding cleft are likely to be charged in the absence of any bound Ca2+ ions, suggests that the net

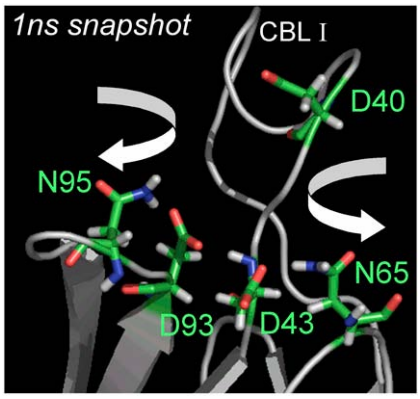

FIGURE 9 Ca^{2+}-binding cleft of the $cPLA_2$ C2 domain in the absence of bound calcium. This structure was generated by replacing Ca^{2+} ions in the binding cleft with water molecules and then carrying out 1 ns of MD. We see that the secondary structure of the binding cleft is essentially unchanged. The large negative potential in the binding cleft created as a result of the removal of the two crystallographically resolved Ca^{2+} ions is released via three well-defined side-chain motions: χ-angle rotations (indicated) of the aspargines Asn-65 and -95 and a movement of Asp-40 away from the binding cleft.

charge in the binding cleft increases by 4 eu upon Ca2+ activation. This suggests that electrostatics plays a vital role in triggering membrane insertion.

We thank Prof. Joseph J. Falke for initial discussions on this work.

This work was supported by National Institutes of Health grant GM R01-054651 to H.L.S./E.J., by a Dept. of Energy/Genomes to Life grant to E.J., and by National Institutes of Health grant 2PN2EY016570-02.

REFERENCES

1. Hurley, J. H. 2003. Membrane proteins. Adapting to life at the interface. *Chem. Biol.* 10:2–3.
2. Malmberg, N. J., D. R. Van Buskirk, and J. J. Falke. 2003. Membrane-docking loops of the cPLA$_2$ C2 domain: detailed structural analysis of the protein-membrane interface via site-directed spin-labeling. *Biochem.* 42:13227–13240.
3. Hurley, J. H., and T. Meyer. 2001. Subcellular targeting by membrane lipids. *Curr. Opin. Cell Biol.* 13:146–152.
4. Tomsig, J. L., and C. E. Creutz. 2002. Copines: a ubiquitous family of Ca^{2+}-dependent phospholipid-binding proteins. *Cell. Mol. Life Sci.* 59: 1467–1477.
5. Kohout, S. C., S. Corbalan-Garcia, A. Torrecillas, J. C. Gomez-Fernandez, and J. J. Falke. 2002. C2 domains of protein kinase C isoforms alpha, beta, and gamma: activation parameters and calcium stoichiometries of the membrane-bound state. *Biochem.* 41:11411–11424.
6. Nalefski, E. A., M. A. Wisner, J. Z. Chen, S. R. Sprang, M. Fukuda, K. Mikoshiba, and J. J. Falke. 2001. C2 domains from different Ca^{2+} signaling pathways display functional and mechanistic diversity. *Biochem.* 40:3089–3100.
7. Nalefski, E. A., and J. J. Falke. 1996. The C2 domain calcium-binding motif: structural and functional diversity. *Prot. Sci.* 5:2375–2390.
8. Cho, W. 2001. Membrane targeting by C1 and C2 domains. *J. Biol. Chem.* 276:32407–32410.
9. Rotin, D., O. Staub, and R. Haguenauer-Tsapis. 2000. Ubiquitination and endocytosis of plasma membrane proteins: role of Nedd4/Rsp5p family of ubiquitin-protein ligases. *J. Membr. Biol.* 176:1–17.
10. Edwards, A. S., and A. C. Newton. 1997. Regulation of protein kinase Cβ II by its C2 domain. *Biochem.* 36:15615–15623.
11. Sutton, R. B., B. A. Davletov, A. M. Berghuis, T. C. Sudhof, and S. R. Sprang. 1995. Structure of the first C2 domain of synaptotagmin I: a novel Ca^{2+}/phospholipid-binding fold. *Cell.* 80:929–938.
12. Perisic, O., S. Fong, D. E. Lynch, M. Bycroft, and R. L. Williams. 1998. Crystal structure of a calcium-phospholipid binding domain from cytosolic phospholipase A$_2$. *J. Biol. Chem.* 273:1596–1604.
13. Sutton, R. B., and S. R. Sprang. 1998. Structure of the protein kinase Cβ phospholipid-binding C2 domain complexed with Ca^{2+}. *Structure.* 6:1395–1405.
14. Shao, X., I. Fernandez, T. C. Sudhof, and J. Rizo. 1998. Solution structures of the Ca^{2+}-free and Ca^{2+}-bound C2A domain of synaptotagmin I: does Ca^{2+} induce a conformational change? *Biochem.* 37:16106–16115.
15. Davletov, B., O. Perisic, and R. L. Williams. 1998. Calcium-dependent membrane penetration is a hallmark of the C2 domain of cytosolic phospholipase A$_2$ whereas the C2A domain of synaptotagmin binds membranes electrostatically. *J. Biol. Chem.* 273:19093–19096.
16. Xu, G. Y., T. McDonagh, H. A. Yu, E. A. Nalefski, J. D. Clark, and D. A. Cumming. 1998. Solution structure and membrane interactions of the C2 domain of cytosolic phospholipase A$_2$. *J. Mol. Biol.* 280: 485–500.
17. Dessen, A., J. Tang, H. Schmidt, M. Stahl, J. D. Clark, J. Seehra, and W. S. Somers. 1999. Crystal structure of human cytosolic phospholipase A$_2$ reveals a novel topology and catalytic mechanism. *Cell.* 97: 349–360.
18. Essen, L. O., O. Perisic, D. E. Lynch, M. Katan, and R. L. Williams. 1997. A ternary metal binding site in the C2 domain of phosphoinositide-specific phospholipase C-δ1. *Biochem.* 36:2753–2762.
19. Nalefski, E. A., M. M. Slazas, and J. J. Falke. 1997. Ca^{2+}-signaling cycle of a membrane-docking C2 domain. *Biochem.* 36:12011–12018.
20. Ubach, J., X. Zhang, X. Shao, T. C. Sudhof, and J. Rizo. 1998. Ca^{2+} binding to synaptotagmin: how many Ca^{2+} ions bind to the tip of a C2-domain? *EMBO J.* 17:3921–3930.
21. Murray, D., and B. Honig. 2002. Electrostatic control of the membrane targeting of C2 domains. *Mol. Cell.* 9:145–154.
22. Verdaguer, N., S. Corbalan-Garcia, W. F. Ochoa, I. Fita, and J. C. Gomez-Fernandez. 1999. Ca^{2+} bridges the C2 membrane-binding domain of protein kinase Cα directly to phosphatidylserine. *EMBO J.* 18:6329–6338.
23. Conesa-Zamora, P., M. J. Lopez-Andreo, J. C. Gomez-Fernandez, and S. Corbalan-Garcia. 2001. Identification of the phosphatidylserine binding site in the C2 domain that is important for PKC alpha activation and in vivo cell localization. *Biochem.* 40:13898–13905.
24. Ochoa, W. F., S. Corbalan-Garcia, R. Eritja, J. A. Rodriguez-Alfaro, J. C. Gomez-Fernandez, I. Fita, and N. Verdaguer. 2002. Additional binding sites for anionic phospholipids and calcium ions in the crystal structures of complexes of the C2 domain of protein kinase Cα. *J. Mol. Biol.* 320:277–291.
25. Bolsover, S. R., J. C. Gomez-Fernandez, and S. Corbalan-Garcia. 2003. Role of the Ca^{2+}/phosphatidylserine binding region of the C2 domain in the translocation of protein kinase Cα to the plasma membrane. *J. Biol. Chem.* 278:10282–10290.
26. Zhang, X., J. Rizo, and T. C. Sudhof. 1998. Mechanism of phospholipid binding by the C2A-domain of synaptotagmin I. *Biochem.* 37:12395–12403.
27. Nalefski, E. A., and J. J. Falke. 1998. Location of the membrane-docking face on the Ca2+-activated C2 domain of cytosolic phospholipase A$_2$. *Biochem.* 37:17642–17650.
28. Malmberg, N. J., S. Varma, E. Jakobsson, and J. J. Falke. 2004. Ca^{2+} activation of the cPLA2 C2 domain: ordered binding of two Ca^{2+} ions with positive cooperativity. *Biochem.* 43:16320–16328.
29. Nalefski, E. A., T. McDonagh, W. Somers, J. Seehra, J. J. Falke, and J. D. Clark. 1998. Independent folding and ligand specificity of the C2 calcium-dependent lipid binding domain of cytosolic phospholipase A$_2$. *J. Biol. Chem.* 273:1365–1372.
30. Evans, J. H., D. M. Spencer, A. Zweifach, and C. C. Leslie. 2001. Intracellular calcium signals regulating cytosolic phospholipase A$_2$ translocation to internal membranes. *J. Biol. Chem.* 276:30150–30160.
31. Lindahl, E., B. Hess, and D. van der Spoel. 2001. GROMACS: a package for molecular simulation and trajectory analysis. *J Mol. Mod.* 7: 306–313.
32. Jorgensen, W. L., D. S. Maxwell, and J. Tirado-Rives. 1996. Development and testing of the OPLS all-atom force field on conformational energetics and properties of organic liquids. *J. Am. Chem. Soc.* 118: 11225–11236.
33. Dolinsky, T. J., J. E. Nielsen, J. A. McCammon, and N. A. Baker. 2004. PDB2PQR: an automated pipeline for the setup of Poisson-Boltzmann electrostatics calculations. *Nucleic Acids Res.* 32:W665–W667.
34. Hoover, W. G. 1985. Canonical dynamics: equilibrium phase-space distributions. *Phys. Rev. A.* 31:1695–1697.
35. Parrinello, M., and A. Rahman. 1981. Polymorphic transition in single crystals: a new molecular dynamics method. *J. Appl. Phys.* 52:7128–7190.
36. Hess, B., H. Bekker, H. J. Berendsen, and G. E. M. Fraaije. 1997. LINCS: a linear constraint solver for molecular simulations. *J Comp. Chem.* 18:1463–1472.
37. Miyamoto, S., and P. Kollman. 1992. SETTLE: an analytical version of the SHAKE and RATTLE algorithms for rigid water molecules. *J Comp. Chem.* 13:952–962.

38. Fiorin, G., R. R. Biekofsky, A. Pastore, and P. Carloni. 2005. Unwinding the helical linker of calcium-loaded calmodulin: a molecular dynamics study. *Proteins*. 61:829–839.

39. Berendsen, H. J., J. P. M. Postma, W. F. van Gunsteren, and J. Hermans. 1981. Intermolecular Forces. Reidel, Dordrecht, The Netherlands.

40. Berendsen, H. J., J. R. Grigera, and T. P. Straatsma. 1987. The missing term in effective pair potentials. *J. Phys. Chem*. 91:6269–6271.

41. Jorgensen, W. L., and J. D. Madura. 1985. Temperature and size dependence for Monte Carlo simulations of TIP4P water. *Mol. Phys*. 56:1381–1392.

42. Kusalik, P. G., and I. M. Svishchev. 1994. The spatial structure in liquid water. *Science*. 265:1219–1221.

43. van der Spoel, D., P. J. van Maaren, and H. J. Berendsen. 1998. A systematic study of water models for molecular simulation: derivation of water models optimized for use with a reaction field. *J. Phys. Chem*. 108:10220–10230.

44. Mahoney, M. W., and W. L. Jorgensen. 2000. A five-site model for liquid water and the reproduction of the density anomaly by rigid, nonpolarizable potential functions. *J. Chem. Phys*. 112:8910–8922.

45. Mahoney, M. W., and W. L. Jorgensen. 2001. Diffusion constant of the TIP5P model of liquid water. *J. Chem. Phys*. 114:363–366.

46. Guillot, B. 2002. A reappraisal of what we have learnt during three decades of computer simulations on water. *J. Mol. Liq*. 101:219–260.

47. Daggett, V., and M. Levitt. 1992. Molecular dynamics simulations of helix denaturation. *J. Mol. Biol*. 223:1121–1138.

48. Avbelj, F., P. Luo, and R. L. Baldwin. 2000. Energetics of the interaction between water and the helical peptide group and its role in determining helix propensities. *Proc. Natl. Acad. Sci. USA*. 97:10786–10791.

49. Vila, J. A., D. R. Pipoll, and H. A. Scheraga. 2000. Physical reasons for the unusual alpha-helix stabilization afforded by charged or neutral polar residues in alanine-rich peptides. *Proc. Natl. Acad. Sci. USA*. 97:13075–13079.

50. Garcia, A. E., and K. Y. Sanbonmatsu. 2002. α-Helical stabilization by side chain shielding of backbone hydrogen bonds. *Proc. Natl. Acad. Sci. USA*. 99:2782–2787.

51. Walsh, S. T. R., R. P. Cheng, W. W. Wright, D. O. V. Alonso, V. Daggett, J. M. Vanderkooi, and W. F. DeGrado. 2003. The hydration of amides in helices; a comprehensive picture from molecular dynamics, IR, and NMR. *Prot. Sci*. 12:520–531.

52. Banci, L., G. Cavallaro, V. Kheifets, and D. Mochly-Rosen. 2002. Molecular dynamics characterization of the C2 domain of protein kinase Cβ. *J. Biol. Chem*. 277:12988–12997.

53. Romero, P., Z. Obradovic, and A. K. Dunker. 2004. Natively disordered proteins: functions and predictions. *Appl. Bioinformatics*. 3:105–113.

54. Radivojac, P., S. Vucetic, T. R. O'Connor, V. N. Uversky, Z. Obradovic, and A. K. Dunker. 2006. Calmodulin signaling: analysis and prediction of a disorder-dependent molecular recognition. *Proteins: Strut. Func. & Gen*. 63:398–410.

55. Varma, S., and E. Jakobsson. 2004. Ionization states of residues in OmpF and mutants: effects of dielectric constant and interactions between residues. *Biophys. J*. 86:690–704.